Band-Rejection Feedback for Chaotic Time-Delay Signature Suppression in a Semiconductor Laser

Song-Sui Li, *Member, IEEE*, Xihua Zou, *Senior Member, IEEE*, Liyue Zhang, Lin Jiang, Longsheng Wang, Anbang Wang, Wei Pan, and Lianshan Yan

***Abstract*—Chaos generation from a semiconductor laser under band-rejection optical feedback is proposed and investigated numerically and experimentally. The band-rejection feedback performs better than the conventional broadband mirror feedback in concealing the feedback delay time information measured by the time-delay signature (TDS) of optical field and intensity. In this work, the optical band-rejection filter (BRF) is built up based on the transmission of a Bragg grating. The best concealment of delay time information is achieved in the form of simultaneous TDS suppression in optical field and intensity when the BRF is negatively detuned from the free-running laser frequency. Such concealment is due to the suppression of feedback cavity modes by the band-rejection effect. The concealment prefers negative detuning frequency because the laser cavity resonance is red-shifted by optical feedback due to the antiguidance effect. The negatively detuned BRF suppresses the TDS of optical field and intensity by more than an order of magnitude than mirror feedback. The simulation results are qualitatively confirmed by the experimental measurements.**

***Index Terms*—Band-rejection filter (BRF), chaos, optical feedback, semiconductor laser, time-delay signature (TDS).**

I. Introduction

OPTICAL chaos from semiconductor lasers are of particular interest due to unique properties such as broad bandwidth, noise-like but synchronizable waveform, and high dimension [1]–[6]. Chaotic laser dynamics have inspired a number of novel applications including chaotic secure communication and key distribution [1], [4], [7], [8], ultra-fast random bit generation [3], [9], [10], chaotic ranging [11], [12], and photonic information processing [5], [13]. Nonlinear dynamics of semiconductor lasers can be realized by using external perturbations such as optical injection, optoelectronic feedback, and optical feedback. Optical feedback can excite locking dynamics for semiconductor lasers to enhance the coherence quality and modulation bandwidth in optical communications [14]–[19]. It has also been demonstrated to stabilize the mode-locking dynamics [20], [21]. Using optical feedback is one of the most popular approaches as it provides a wide parameter space for chaos generation by simply involving only one laser [22], [23]. Chaotic dynamics from a feedback scheme inherently contains an information about the characteristic delay time within the external feedback cavity. Such a delay time information results in a weak periodic property in both intensity and phase dynamics, which can be extracted by using information processing techniques such as time-dependent exponent, neural network analysis, permutation entropy, delayed mutual information (DMI), or autocorrelation function (ACF) [24]–[27]. Measuring the ACF of time series is the most straightforward way as the delay time information can be converted to a local correlation peak with high computational efficiency [28]–[30]. Such correlation peak is known as the time-delay signature (TDS), which discloses the characteristic delay time in chaos generation and is often undesirable for chaos-based applications, as it weakens the security in chaos communication or key distribution, reduces the randomness in bit generation, and impairs the precision in target detection [2], [22]. As a result, suppression of TDS from both intensity and phase dynamics is necessary.

In the last decade, a lot of efforts have been done to solve the TDS problem. Amongst the state-of-the-art approaches, using modifications on feedback cavity has received massive investigation as it combines TDS suppression to chaos generation. For suppressing the TDS in intensity dynamics, the pioneer approach was numerically demonstrated using mirror feedback, where the intensity TDS was covered by the lasers relaxation resonance under short delay [24]. A few years later, this technique was experimentally demonstrated by using on-chip integrated feedback [31], [32]. Besides single-loop feedback, multi-loop feedback have been studied for intensity TDS suppression as well [33], [34]. As an extension of polarization-matched feedback, polarization rotation was included in the feedback cavity, where the intensity TDS was suppressed due to the reduced coherence between the internal and feedback fields [35], [36]. Besides using feedback cavity with identical delay, approaches

Manuscript received January 9, 2022; revised February 15, 2022; accepted February 19, 2022. Date of publication February 23, 2022; date of current version March 11, 2022. This work was supported in part by the National Key Research and Development Program of China under Grant 2019YFB1803500, in part by the National Natural Science Foundation of China under Grants 61905204 and 62005228, in part by the Major Key Project of PCL under Grant PCL2021A14, in part by the Sichuan Science and Technology Program under Grant 2020YJ0014, and in part by the Fundamental Research Funds for the Central Universities under Grant 2682020CX82. *(Corresponding author: Song-Sui Li.)*

Song-Sui Li, Xihua Zou, Liyue Zhang, Lin Jiang, and Wei Pan are with the School of Information Science and Technology, Southwest Jiaotong University, Chengdu 610031, China (e-mail: ssli@swjtu.edu.cn; zouxihua@swjtu.edu.cn; liyuezhang1989@126.com; linjiang@swjtu.edu.cn; wpan@swjtu.edu.cn).

Longsheng Wang and Anbang Wang are with the College of Physics and Optoelectronics, Taiyuan University of Technology, Taiyuan 030024, China, and with the Key Lab of Advanced Transducers and Intelligent Control System, Ministry of Education, Taiyuan University of Technology, Taiyuan 030024, China (e-mail: wanglongsheng@tyut.edu.cn; wanganbang@tyut.edu.cn).

Lianshan Yan is with the School of Information Science and Technology, Southwest Jiaotong University, Chengdu 610031, China, and with the Peng Cheng Laboratory, Shenzhen 518052, China (e-mail: lsyan@swjtu.edu.cn).

Digital Object Identifier 10.1109/JPHOT.2022.3153640

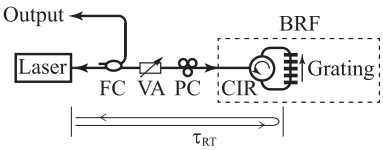

Fig. 1. Setup of a semiconductor laser under band-rejection optical feedback. FC, fiber coupler; VA, variable attenuator; PC, polarization controller; CIR, optical circulator; BRF, band-rejection filter; τ_{RT}, feedback round-trip delay time.

using dispersive feedback cavity were also numerically and experimentally demonstrated, where the intensity TDS was flattened and suppressed due to the group-velocity dispersion [37]–[42]. Despite being suppressed in intensity dynamics, the TDS was numerically predicted from phase dynamics [43], [44]. For further suppressing the TDS in phase dynamics, the most popular method involves phase scrambling in the feedback cavity [45], [46]. Nonetheless, phase modulation often increases the system complexity. Filtered optical feedback is a much simpler approach towards perturbing both intensity and phase dynamics. Optical feedback using band-pass filter was demonstrated by Fischer *et al*. [47]. Band-pass filter usually suppresses the side bands of coherence collapse, hence is more helpful for stabling periodic dynamics [48], [49]. As a supplement of band-pass feedback, band-rejection feedback may keep such side bands, hence its effect towards chaos generation is worth investigating.

In this paper, a novel approach for concealing delay time information is proposed by using band-rejection optical feedback. The band-rejection filter (BRF) effectively suppresses the feedback cavity modes hence conceals the delay time information in the form of simultaneous TDS suppression in intensity and phase dynamics. The enhancements are further investigated by varying feedback and BRF parameters. Following this introduction, the model is presented in Section II. The results are described in Section III. A conclusion follows them in Section IV.

II. Setup

The setup in Fig. 1 describes a semiconductor laser subject to optical feedback from a BRF. The BRF consists of an optical circulator and a fiber Bragg grating (FBG), and it provides band-rejection effect by making use of the transmission of grating. The laser is described by the normalized intracavity slowly-varying optical field amplitude $a(t)$ and charge-carrier density $\tilde{n}(t)$ in reference to the free running. Using $h(t)$ as the impulse response of the transmission of Bragg grating and $\Delta\Omega = 2\pi\Delta f$ as the angular frequency detuning of the Bragg frequency away from the laser free-running frequency, the light fed back to the laser is proportional to a convolution, $\left[h(t)e^{-\mathrm{i}\Delta\Omega \mathrm{t}}\right] * a(t-\tau_{\mathrm{RT}})$, where τ_{RT} is the round-trip delay time of feedback loop excluding the grating. The rate equations that govern the laser dynamics are [50], [51]:

$$\begin{aligned}\frac{\mathrm{d}a}{\mathrm{d}t} = &\frac{1-\mathrm{i}b}{2\gamma_{\mathrm{s}}\tilde{J}}\left[\gamma_{\mathrm{c}}\gamma_{\mathrm{n}}\tilde{n} - \gamma_{\mathrm{p}}\gamma_{\mathrm{s}}\tilde{J}(|a|^2-1)\right]a \\ &+ \gamma_{\mathrm{c}}\xi_{\mathrm{f}}e^{\mathrm{i}\theta}\left[h(t)e^{-\mathrm{i}\Delta\Omega \mathrm{t}}\right] * a(t-\tau_{\mathrm{RT}}), \qquad (1)\end{aligned}$$

$$\begin{aligned}\frac{\mathrm{d}\tilde{n}}{\mathrm{d}t} = &-\gamma_{\mathrm{s}}\tilde{n} - \gamma_{\mathrm{s}}\tilde{J}(|a|^2-1) \\ &-\frac{1}{\gamma_{\mathrm{c}}}\left[\gamma_{\mathrm{c}}\gamma_{\mathrm{n}}\tilde{n} - \gamma_{\mathrm{p}}\gamma_{\mathrm{s}}\tilde{J}(|a|^2-1)\right]|a|^2, \qquad (2)\end{aligned}$$

where the cavity decay rate $\gamma_{\mathrm{c}} = 5.36\times10^{11}\ \mathrm{s}^{-1}$, the spontaneous carrier relaxation rate $\gamma_{\mathrm{s}} = 5.96\times10^{9}\ \mathrm{s}^{-1}$, the differential carrier relaxation rate $\gamma_{\mathrm{n}} = 7.53\times10^{9}\ \mathrm{s}^{-1}$, the nonlinear carrier relaxation rate $\gamma_{\mathrm{p}} = 1.91\times10^{10}\ \mathrm{s}^{-1}$, the normalized bias current above threshold $\tilde{J} = 1.222$, the linewidth enhancement factor $b = 3.2$, the feedback phase $\theta = 0$, and the feedback strength ξ_{f}. The laser parameters are measured from a 1.3-μm multiple-quantum-well DFB laser (Bookham Technology LC131) at bias current of 40 mA with an output power of about 4.5 mW. The parameters correspond to a relaxation oscillation frequency of $f_{\mathrm{r}} = (2\pi)^{-1}\sqrt{\gamma_{\mathrm{c}}\gamma_{\mathrm{n}} + \gamma_{\mathrm{s}}\gamma_{\mathrm{p}}} \approx 10.25$ GHz [52]. For the feedback term at the right-hand side of (1), the impulse response $h(t)$ is obtained from an inverse Fourier transform of the grating transmission frequency response $H(\Omega)$ which is described as follows [53], [54]:

$$H(\Omega) = \alpha\left[\alpha\cosh(\alpha l) + \mathrm{i}\delta\sinh(\alpha l)\right]^{-1}, \qquad (3)$$

where $\alpha = \sqrt{\kappa^2 - \delta^2}$. $\delta = -n_{\mathrm{eff}}\Omega/c$ and Ω denotes the angular frequency detuning away from the Bragg resonance. $c = 3\times10^{8}\ \mathrm{m/s}$ is the speed of light in vacuum, $n_{\mathrm{eff}} = 1.45$ is the effective refractive index of grating, $l = 0.02$ m is the length of grating, and κ is the coupling coefficient along l.

It can be obtained from (3) that the BRF has a minimum transmission of $1 - \tanh^2(\kappa l)$ at the Bragg frequency of $\Omega = 0$. For a highly reflective grating, the main lobe of BRF has a 3-dB bandwidth roughly equalling to $f_{\mathrm{BW}} = c\kappa/(\pi n_{\mathrm{eff}})$. As for mirror feedback, the impulse response $h(t)$ can be set to $\delta(t)$ and the rate equations in (1)–(2) are reduced to the well-know Lang-Kobayashi model [50]. In this work, the long feedback cavity regime is considered, thus chaotic states instead of self-injection locking states are guaranteed when sufficient feedback strength is adopted. Numerical simulations are conducted using the fourth-order Runge-Kutta method with time step 2.38 ps for time span of 1.25 μs.

III. Numerical Results

A. Dynamical Mapping

Fig. 2 plots the mapping of the dynamical states of the laser in the feedback parameter space $(\Delta f, \xi_{\mathrm{f}})$, where the round-trip delay time is fixed at $\tau_{\mathrm{RT}} = 0.47$ ns and the BRF has a bandwidth of $f_{\mathrm{BW}} = 24$ GHz. By varying the feedback parameters, the stable states (white), period-one states (red), quasi-periodic states (gray), period-doubled states (yellow), and chaotic states (black) are identified according to the distribution of the intensity-time series extrema [37]. For example, when increasing feedback strength ξ_{f} from zero at detuning frequency of $\Delta f = -30$ GHz, the dynamical state evolves from the stable state, period-one state, quasi-periodic state, to the chaotic state. Such a quasi-periodic route-to-chaos is popular in lasers under feedbacks [2], [22]. Moreover, for inducing instability, stronger ξ_{f} is required at about $\Delta f = 0$ due to significant band-rejection effect of BRF.

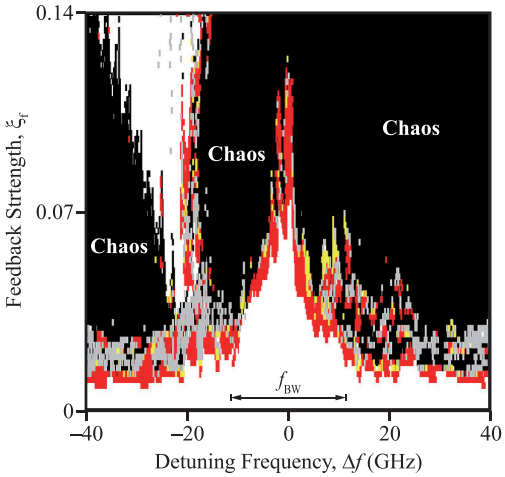

Fig. 2. Numerically calculated mapping of the dynamical states when $f_{\mathrm{BW}} = 24$ GHz. Regions of stable states (white), P1 states (red), quasi-periodic states (gray), period-doubled states (yellow), and chaotic states (black) are identified. $\tau_{\mathrm{RT}} = 0.47$ ns.

Furthermore, different from conventional mirror feedback, a region of stable states is observed under relatively strong ξ_{f} at negative Δf due to locking the red-shifted laser cavity resonance to one of the BRF side lobes. Such red-shifted resonance is induced by optical feedback through the antiguidance effect, which leads to an asymmetry of dynamical mapping with respect to Δf [51]. Most importantly, three large chaotic regions are labeled in the feedback parameter space $(\Delta f, \xi_{\mathrm{f}})$, which reveals the flexibility of chaos generation. Varying Δf from negative to positive values, the three chaotic regions are respectively achieved roughly by making using of the higher frequency side lobes, main lobe, and lower frequency side lobes of the BRF. The rest of this work focuses on the chaotic dynamics.

B. Chaotic Time-Delay Signature

Fig. 3 investigates the optical field amplitude of chaos by plotting the optical spectra and ACF of optical field in columns (i) and (ii), respectively. Figs. 3(b)–3(d) respectively show the data from BRF feedback with different detuning frequencies of $\Delta f = 37$ GHz, -7.5 GHz, and -37 GHz. Fig. 3(a) shows the data from mirror feedback for a comparison. Black curves in column (i) represent optical spectrum of chaos, while green curves represent magnitude-squared frequency responses of mirror or BRF. The round-trip delay time is $\tau_{\mathrm{RT}} = 0.47$ ns for BRF feedback and $\tau_{\mathrm{RT}} = \tau_l + 0.47$ ns for mirror feedback to achieve similar length of optical path within one round trip, where $\tau_l = n_{\mathrm{eff}} l/c \approx 0.10$ ns is the time of flight along the grating length l. The feedback strength is $\xi = 0.10$ for both the mirror and BRF feedback. The BRF bandwidth is $f_{\mathrm{BW}} = 24$ GHz. The optical spectrum is obtained using the Fourier transform of the complex field amplitude $a(t)$. The ACF of optical field is a measure of how well the optical field $a(t)$ matches its delayed replica $a(t-\tau)$, thus it can effectively reflect the correlation properties of the phase dynamics.

For mirror feedback, in Fig. 3(a-i), the green curve shows a flat response as the mirror are broadband without frequency selectivity. The black curve shows a chaotic optical spectrum spanning

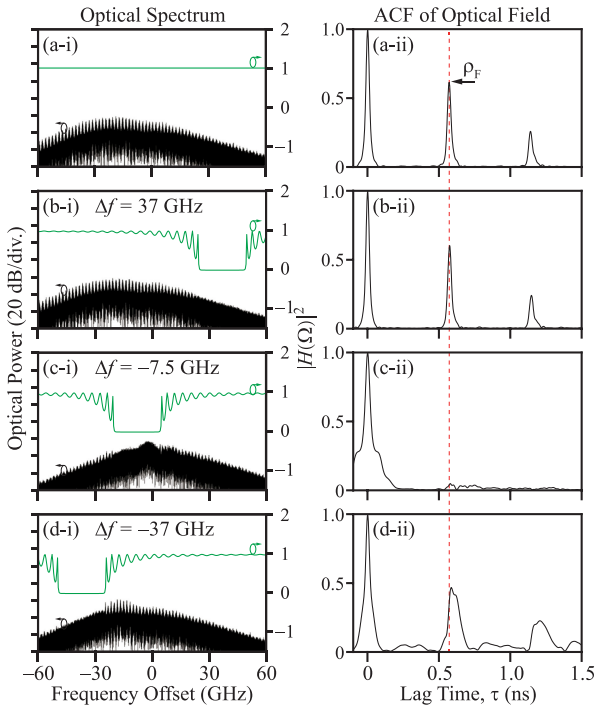

Fig. 3. Numerically calculated (i) optical spectrum and (ii) ACF of optical field, where chaos is generated from (a) mirror feedback and (b)–(d) BRF feedback with Δf of 37 GHz, -7.5 GHz, and -37 GHz, respectively. $\xi_{\mathrm{f}} = 0.10$. $f_{\mathrm{BW}} = 24$ GHz.

a frequency range of over 10 GHz due to coherence collapse by optical feedback [55]. The asymmetry of optical spectrum with respect to the laser free-running frequency is attributed to the red-shifted laser cavity resonance [56]. However, periodic peaks are observed over the spectrum revealing the feedback cavity modes. Such periodic peaks with a frequency gap of about $1/\tau_{\mathrm{RT}}$ in optical spectrum are converted to correlation peaks separated by about τ_{RT} in the ACF of optical field in Fig. 3(a-ii), which agrees well with the Wiener-Khinchin theorem. The value of peak at $\tau \approx \tau_{\mathrm{RT}}$ is named as the TDS of optical field ρ_{F}, which is about 0.61 in Fig. 3(a-ii).

For BRF feedback with positive detuning frequency of $\Delta f = 37$ GHz, in Fig. 3(b-i), the green curve shows a response of BRF corresponding to the transmission of grating. The central band of chaos basically sees the lower frequency side lobes of BRF where the power rejection effect is weak, thus the BRF is almost transparency to the chaos. Such BRF feedback is roughly equivalent to mirror feedback, hence the optical spectrum and ACF of optical field in Fig. 3(b) are similar to that in Fig. 3(a). By changing the detuning frequency to $\Delta f = -7.5$ GHz, in Fig. 3(c-i), the green curve shows that the main lobe of BRF roughly covers the central band of chaos. The chaos is induced because sufficient ξ_{f} is adopted as shown in Fig. 2. Interestingly, the periodic peaks at the central band of chaos are significantly smoothed, as the band-rejection effect suppresses the feedback cavity modes in the main lobe of BRF. Meanwhile, the corresponding ACF of optical field in Fig. 3(c-ii) shows a significant suppression of ρ_{F}. Comparing to mirror feedback, the negatively detuned BRF suppresses the ρ_{F} by more than twelve times to below 0.05. Further changing the detuning frequency

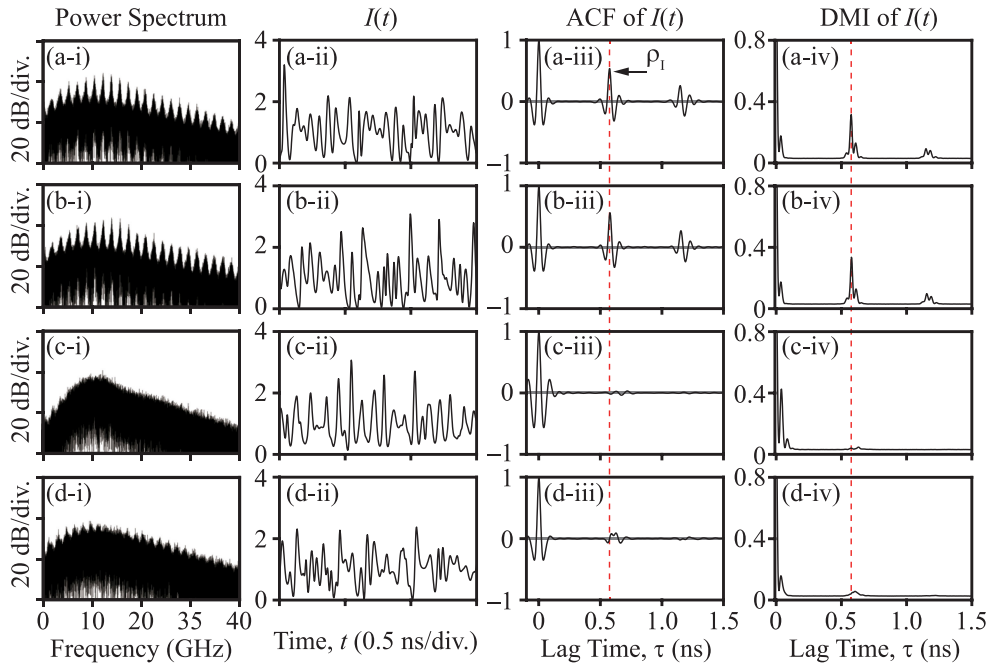

Fig. 4. Numerically calculated (i) power spectrum, (ii) intensity-time series, (iii) ACF of temporal intensity, and (iv) DMI of temporal intensity, where chaos is generated from (a) mirror feedback and (b)–(d) BRF feedback with Δf of 37 GHz, -7.5 GHz, and -37 GHz, respectively. $\xi_{\mathrm{f}} = 0.10$. $f_{\mathrm{BW}} = 24$ GHz.

to $\Delta f = -37$ GHz, in Fig. 3(d-i), the green curve shows that the central band of chaos basically sees the higher frequency side lobes of BRF. Though the periodic peaks are suppresses in the main lobe of BRF, they are still strongly pronounced at the central band of chaos. Thus a clear ρ_{F} is observed in Fig. 3(d-ii). But different from the case in Fig. 3(b-ii), the curve around ρ_{F} is broadened and the ρ_{F} is slightly suppressed due to chromatic dispersion near the main lobe [51].

As mentioned above, the BRF feedback successfully suppresses the ρ_{F}, which reveals a suppression of TDS in phase dynamics. To further study the TDS in intensity dynamics, Figs. 4(a)–4(d) investigate the intensity properties of chaos corresponding to the data in Figs. 3(a)–3(d). Column (ii) plots the intensity-time series $I(t) = |a(t)|^2$, while column (i) plots the power spectra by Fourier-transforming $I(t)$. Columns (iii)–(iv) respectively plot the ACF and DMI of temporal intensity. The DMI is a measure of the information shared by $I(t)$ and its delayed replica $I(t-\tau)$ [24], [51].

For mirror feedback, a broadband power spectrum around f_{r} is observed in Fig. 4(a-i), which corresponds to an intensity-time series randomly fluctuated in a time scale of about $1/f_{\mathrm{r}}$ in Fig. 4(a-ii). Again, periodic peaks with a frequency gap of about $1/\tau_{\mathrm{RT}}$ are observed revealing the feedback cavity modes from the power spectrum in Fig. 4(a-i). Though such periodic property is not easily extracted from $I(t)$ in Fig. 4(a-ii), it is transformed to correlation peaks roughly separated by τ_{RT} in the ACF of temporal intensity in Fig. 4(a-iii) as supported by the Wiener-Khinchin theorem. The value of peak at $\tau \approx \tau_{\mathrm{RT}}$ is named as the TDS of temporal intensity ρ_{I}, which is about 0.54 in Fig. 4(a-iii). In addition, the delay time information identified by ρ_{I} agrees well with the mutual information peak in Fig. 4(a-iv). Besides, the small side peak at $\tau \approx 0.5/f_{\mathrm{r}}$ in Fig. 4(a-iv) corresponds the small autocorrelation trough at $\tau \approx 0.5/f_{\mathrm{r}}$ in Fig. 4(a-iii), which basically reveals the lasers relaxation oscillation. For BRF feedback with positive detuning frequency of $\Delta f = 37$ GHz in Fig. 4(b), similar intensity properties are observed comparing to that in Fig. 4(a), as the BRF feedback is roughly equivalent to mirror feedback as shown in Fig. 3(b-i). By changing the detuning frequency to $\Delta f = -7.5$ GHz, in Fig. 4(c-i), the power spectrum is still broadband around f_{r} while the periodic peaks are smoothed due to the suppression of the feedback cavity modes as shown in Fig. 3(c-i). The $I(t)$ is still noise like in Fig. 4(c-ii), but the corresponding ACF of temporal intensity shows a significant suppression of ρ_{I} in Fig. 4(c-iii). Comparing to mirror feedback, the negatively detuned BRF suppresses the ρ_{I} by more than thirteen times to below 0.04. The suppression of ρ_{I} is confirmed by the reduction of the mutual information peak in Fig. 4(c-iv). Further changing the detuning frequency to $\Delta f = -37$ GHz, in Fig. 4(d-i), the periodic peaks appear again in the power spectrum but much weaker than that from mirror feedback. In Fig. 4(d-iii), the curve around ρ_{I} is broadened and the ρ_{I} is suppressed due to chromatic dispersion near the main lobe of BRF as shown in Fig. 3(d-i) [51]. The suppression of ρ_{I} is also confirmed by the reduced mutual information peak in Fig. 4(d-iv).

It is worth mentioning that, the feedback configuration for Figs. 3(d) and 4(d) is good at suppression of intensity TDS as it shares the same mechanism with previous works using dispersive feedback [37], [40], [41], [51]. Such mechanism relies on inducing group-velocity dispersion on the fed back light, thus it achieves TDS suppression in intensity dynamics rather than in phase dynamics. Better than the dispersive feedback, the band-rejection configuration for Figs. 3(c) and 4(c) performs suppression of the feedback cavity modes, hence it effectively achieves simultaneous suppression of TDS in both intensity and phase dynamics.

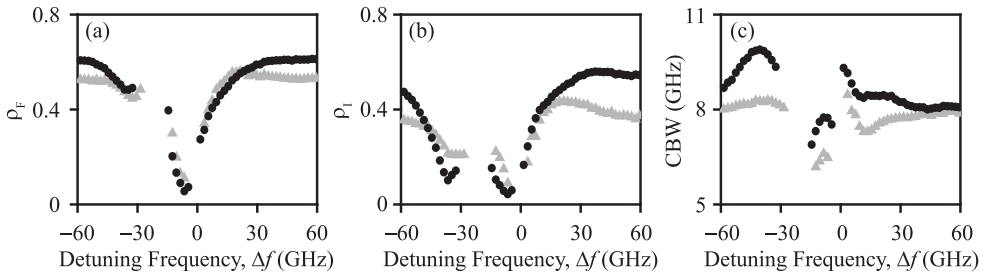

Fig. 5. Numerically calculated (a) ρ_F, (b) ρ_I, and (c) CBW as functions of detuning frequency Δf, where $\xi_f = 0.07$ (triangles) and 0.10 (circles). τ_{RT} =0.47 ns. $f_{BW} = 24$ GHz.

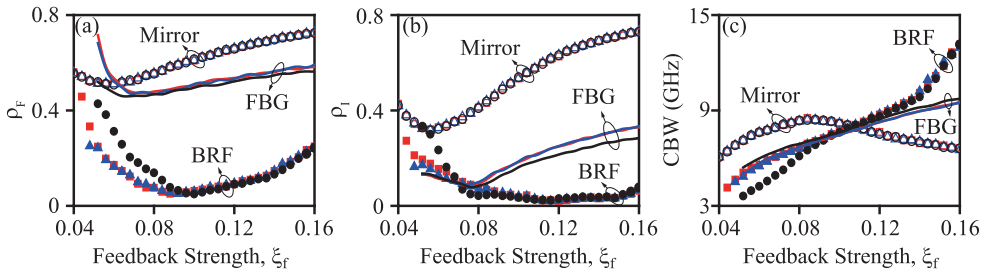

Fig. 6. Numerically calculated (a) ρ_F, (b) ρ_I, and (c) CBW as functions of feedback strength ξ_f. $\Delta f = -7.5$ GHz and 13 GHz for BRF and FBG. $f_{BW} = 24$ GHz for both BRF and FBG. Open symbols, closed symbols, and lines are from mirror, BRF, and FBG feedback, respectively.

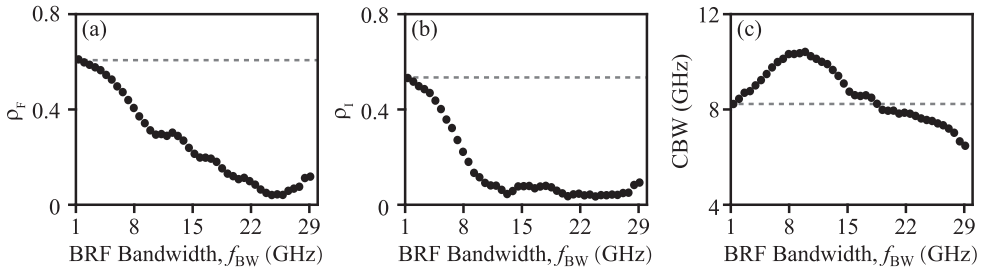

Fig. 7. Numerically calculated (a) ρ_F, (b) ρ_I, and (c) CBW as functions of BRF bandwidth f_{BW}. $\Delta f = -7.5$ GHz. $\xi_f = 0.10$. $\tau_{RT} = 0.47$ ns. Dashed lines are the data of mirror feedback.

C. Dependencies

The above investigation shows that the BRF feedback successfully achieves simultaneous suppression of ρ_F and ρ_I by suppressing the feedback cavity modes using negatively detuned BRF. To detailed study the dependences on parameters, Figs. 5–7 conduct the investigation by varying feedback and BRF parameters.

Figs. 5(a)–5(c) respectively show, as functions of detuning frequency Δf, the ρ_F, ρ_I, and the chaotic bandwidth (CBW). CBW is defined as the effective bandwidth that contains 80% of the total power in the single-sideband power spectrum of the chaos intensity [51], [57]. The feedback strength is fixed at $\xi_f = 0.07$ and 0.10 for triangles and circles, respectively. The round-trip delay time is $\tau_{RT} = 0.47$ ns. The BRF bandwidth is $f_{BW} = 24$ GHz. Starting with the data by circles, the feedback strength is fixed at $\xi_f = 0.10$. As Δf varies, three group of data are observed corresponding to the three chaotic regions labeled in Fig. 2. When $\Delta f < -32$ GHz, the central band of chaos sees the higher frequency side lobes of BRF where the power rejection is relatively weak. As Δf increases within this region, slightly suppression of ρ_F in Fig. 5(a) and significant suppression of ρ_I in Fig. 5(b) are observed at about $\Delta f = -37$ GHz. Because the central band of chaos experiences increased chromatic dispersion when approaching to the main lobe of BRF. Further increasing Δf within this region, both ρ_F and ρ_I increase a little bit before moving out of chaotic region. When -15 GHz$< \Delta f < -4$ GHz, the central band of chaos sees the main lobe of BRF where the power rejection becomes strong. As Δf increases within this region, best suppression of ρ_F and ρ_I are simultaneously achieved at about $\Delta f = -7.5$ GHz. Because the feedback cavity modes within the central band of chaos are significantly suppressed by the main lobe of BRF. Further increasing Δf within this region, both ρ_F and ρ_I increase a little bit before moving out of chaotic region. When $\Delta f >2$ GHz, the central band of chaos starts to

see the lower frequency side lobes of BRF. The asymmetric dependence on Δf is due to the red-shifted resonance by optical feedback. As Δf increases within this region, increments of both ρ_{F} and ρ_{I} are observed. Because the central band of chaos experiences decreased chromatic dispersion when moving away from the main lobe of BRF. Such increments of ρ_{F} and ρ_{I} are saturated when Δf >30 GHz, as the BRF feedback is roughly equivalent to mirror feedback. For the CBW in Fig. 5(c), the variation as a function of Δf is roughly the reverse of that for the ρ_{I}. Generally, CBW is smaller in -15 GHz< $\Delta f < -4$ GHz than in other two regions due to the band-rejection from the main lobe of BRF. Interestingly, best suppression of ρ_{F} and ρ_{I} are achieved at a local maximum of CBW. Globally, the TDS suppression compromises on CBW performance as Δf varies in Fig. 5. Nonetheless, such trade-off can be broken by enhancing the lasers relaxation oscillation frequency f_{r} using higher bias current. Comparing the triangles and circles, the data show that the ρ_{F}, ρ_{I}, and CBW are all sensitive to the feedback strength.

In addition to the detuning frequency, the chaotic dynamics is also investigated by varying the feedback strength ξ_{f}. Figs. 6(a)–6(c) respectively show, as functions of ξ_{f}, the ρ_{F}, ρ_{I}, and CBW. The data from BRF feedback with $\Delta f = -7.5$ GHz are shown by closed symbols where the round-trip delay time is fixed at $\tau_{\mathrm{RT}} = 4.7$ ns, 2.35 ns, and 0.47 ns in red, blue, and black. Besides, the data from mirror feedback are shown by open symbols with $\tau_{\mathrm{RT}} = \tau_l$+4.7 ns, τ_l +2.35 ns, and τ_l +0.47 ns in red, blue, and black. Moreover, the data from FBG feedback with $\Delta f = 13$ GHz are shown by lines with $\tau_{\mathrm{RT}} = 4.7$ ns, 2.35 ns, and 0.47 ns in red, blue, and black. The feedback strength is $\xi_{\mathrm{f}} = 0.10$. The BRF bandwidth is $f_{\mathrm{BW}} = 24$ GHz. Starting with the data by circles, for the open symbols from mirror feedback, both ρ_{F} in Fig. 6(a) and ρ_{I} in Fig. 6(b) are found to first reduce to a local minimum and then increase as ξ_{f} increases. Meanwhile, the CBW in Fig. 6(c) is found to first increase and then reduce as ξ_{f} increases. Here, the CBW is reduced because the feedback cavity modes are enhanced such that the chaos power is condensed in the discrete periodic peaks in power spectrum. For the closed symbols from BRF feedback, similar to mirror feedback, both ρ_{F} in Fig. 6(a) and ρ_{I} in Fig. 6(b) are strongly pronounced at weak ξ_{f}. Better than mirror feedback, the BRF feedback achieves further suppression of both ρ_{F} and ρ_{I} as ξ_{f} increases. Meanwhile, the CBW in Fig. 6(c) is found to increase with ξ_{f} and is even broadener than that from mirror feedback when ξ_{f} >0.10. Nonetheless, the reduction of CBW can be realized if ξ_{f} is sufficient to compensate the band-rejection effect. Comparing to the performance of FBG feedback with optimized detuning frequency, the BRF feedback achieves significant improvement in suppressing the ρ_{F}. Because the FBG provides dispersive feedback to perturb the intensity dynamics, which is less helpful for suppression the TDS in phase dynamics. In addition, the ρ_{F}, ρ_{I}, and CBW from BRF feedback become less sensitive to τ_{RT} as ξ_{f} increases.

In addition to feedback parameters, the chaotic dynamics is further investigated by varying the BRF bandwidth f_{BW} through adjusting the grating coupling coefficient κ. Figs. 7(a)–7(c) respectively show, as functions of f_{BW}, the ρ_{F}, ρ_{I}, and CBW. The detuning frequency is fixed at $\Delta f = -7.5$ GHz. The feedback strength is $\xi_{\mathrm{f}} = 0.10$. The round-trip delay time is $\tau_{\mathrm{RT}} = 0.47$ ns. The dashed lines represent data from mirror feedback for references. When small f_{BW} is adopted by using sufficient weak κ, the ρ_{F} in Fig. 7(a), ρ_{I} in Fig. 7(b), and CBW in Fig. 7(c) are comparable to that of mirror feedback. Because a grating with sufficient weak κ basically is reduced to a piece of fiber, hence the performance is closed to that of mirror feedback. Increasing f_{BW} leads to suppression of both ρ_{F} and ρ_{I}, as the suppression of feedback cavity modes is enhanced by increasing the number of modes covered by the main lobe of BRF. Comparing to mirror feedback, the ρ_{F} and ρ_{I} can be suppressed by more than an order of magnitude without significant reduction of CBW when f_{BW} is about 24 GHz. Further increasing f_{BW} leads to increments of ρ_{F} and ρ_{I}, as the rejection band is too broad to have sufficient feedback for maintaining chaotic oscillations. This is further confirmed by the reduction of CBW in Fig. 7(c).

IV. Experimental Results

The experimental investigation on TDS suppression by BRF feedback is conducted based on the setup in Fig. 1. The 1550-nm DFB laser (KG-DFB-15-10-S-FA) is temperature-stabilized at 29 °C and forward-biased at 13 mA (1.5 times its threshold current). The output power is about 1.7 mW corresponding to a relaxation resonance frequency f_{r} ≈4 GHz. For the BRF, the grating is a commercially available uniform FBG centered at 1550 nm with a 3-dB bandwidth of about 0.2 nm (f_{BW} ≈25 GHz). The circulator has 58-dB isolation to avoid reflection from the grating. The feedback fiber loop has a total length of about 8.87 m which gives the external cavity round-trip time of $\tau_{\mathrm{RT}} = 43.5$ ns. For analyzing the output, the coupler directs 10% power to the optical amplifier (Amonics AEDFA-PA-35) and the photodetector (u ^{2} t XPDV2120RA). The output electrical signal is monitored by the power spectrum analyzer of 7-GHz bandwidth (Rohde & Schwarz FSVR). In the experiments, the feedback strength ξ_{f} is controlled by the fiber based variable attenuator. It is proportional to the square root of the ratio of feedback power to emission power. To avoid unwanted phase variation from the grating, the detuning frequency Δf is adjusted by varying the laser free-running frequency through temperature-tuning with a slop of about 11 GHz/°C.

Figs. 8(a) and 8(b) respectively plot the power spectrum and corresponding ACF of temporal intensity for $\Delta f = 40$ GHz (black) and -4 GHz (red) when $\xi_{\mathrm{f}} = 0.115$. The noise floor in Fig. 8(a) is shown in gray for a reference. Fig. 8(c) further verifies the dependences of TDS on feedback parameters, where ρ_{I} as a function of Δf at $\xi_{\mathrm{f}} = 0.115$ are shown by closed symbols and as a function of ξ_{f} at $\Delta f = -4$ GHz are shown by open symbols. In Fig. 8(a), the power spectra are measured with a resolution bandwidth of 1 MHz. Under $\Delta f = 40$ GHz where the BRF is almost transparency to the chaos, the black curve shows a broadband spectrum with clear feedback cavity modes gapped by about 23 MHz in the inset. Such periodic cavity modes are transformed to correlation peaks roughly separated by about 43.5 ns in the ACF of temporal intensity in Fig. 8(b-i) as supported by the Wiener-Khinchin theorem. The measured ρ_{I} is about 0.62. Interestingly, when $\Delta f = -4$ GHz where the

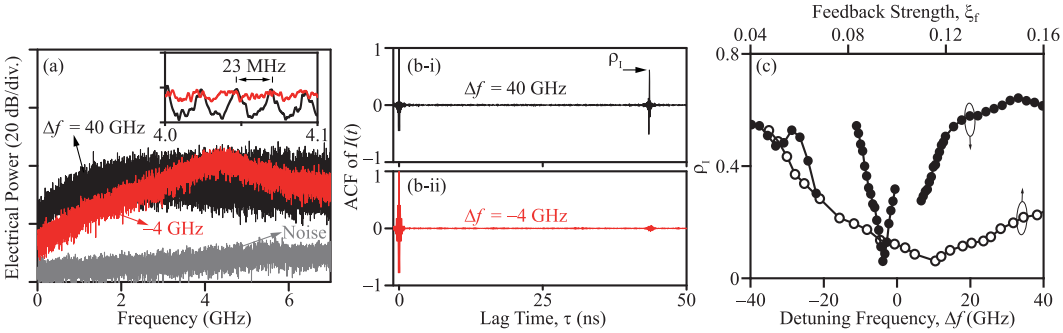

Fig. 8. Experimentally measured (a) power spectrum, (b) autocorrelation, and (c) ρ_{I} as functions of feedback parameters.

BRF induces considerable power attenuation to the central band of chaos, the red curve also shows a broadband spectrum but the feedback cavity modes are significantly smoothed in the inset. As expected, the ρ_{I} is significantly suppressed down to about 0.06 in Fig. 8(b-ii). The suppression of TDS using main lobe of BRF qualitatively agrees well with the simulation results.

To verify the dependences on Δf, the ρ_{I} are recorded by closed symbols in Fig. 8(c). Interestingly, comparing to the simulation results in Fig. 5(b), similar asymmetric dependences on Δf are observed. For instance, when $\Delta f < -22$ GHz, the chaos sees the higher frequency side lobes of BRF. As Δf increases within this region, suppression of ρ_{I} are observed. Further increasing Δf, the laser is pushed out of chaotic region. When -11 GHz$< \Delta f < -1$ GHz, the chaos sees the main lobe of BRF where the power rejection becomes strong. As Δf increases within this region, best suppression of ρ_{I} are achieved at about $\Delta f = -4$ GHz. Further increasing Δf within this region, ρ_{I} increases before moving out of chaotic region. When $\Delta f >$6 GHz, the chaos starts to see the lower frequency side lobes of BRF. As Δf increases within this region, increment of ρ_{I} is observed. Such increment is saturated when $\Delta f >$40 GHz, as the BRF feedback is roughly equivalent to mirror feedback. To verify the dependences on ξ_{f}, the ρ_{I} are recorded by open symbols in Fig. 8(c). Again, comparing to the simulation results in Fig. 6(b), similar dependences on ξ_{f} are observed. The experimental results show that the dependences of ρ_{I} on Δf and ξ_{f} qualitatively agree well with the simulation results. The results and analysis of simulations and experiments are based on DFB lasers with quantum-well structure, while the effects on other type of semiconductor lasers with lower active region dimensionality, such as quantum-wire or quantum-dot lasers, are necessary to be further investigated in the future work.

V. Conclusion

In conclusion, we have proposed and demonstrated a novel approach towards chaotic time-delay signature suppression using optical feedback from a BRF numerically and experimentally. The BRF is achieved by making use of the transmission of a Bragg grating. Regions of chaotic state are observed in the feedback parameter space, which guarantee the flexibility for chaos generation. When the central band of chaos is covered by the main lobe of BRF through using a negatively detuned BRF with proper bandwidth, the TDS of optical field ρ_{F} and TDS of temporal intensity ρ_{I} are effectively suppressed due to suppression of the feedback cavity modes. Comparing to conventional mirror feedback, the negatively detuned BRF simultaneously suppresses the ρ_{F} and ρ_{I} by more than an order of magnitude. Experimental verifications qualitatively agree well with the simulations.

References

[1] A. Argyris *et al.*, "Chaos-based communications at high bit rates using commercial fibre-optic links," *Nature*, vol. 438, pp. 343–346, Nov. 2005.
[2] M. Sciamanna and K. A. Shore, "Physics and applications of laser diode chaos," *Nature Photon.*, vol. 9, pp. 151–162, 2015.
[3] A. Uchida *et al.*, "Fast physical random bit generation with chaotic semiconductor lasers," *Nature Photon.*, vol. 2, pp. 728–732, Dec. 2008.
[4] O. Spitz *et al.*, "Private communication with quantum cascade laser photonic chaos," *Nature Commun.*, vol. 12, 2021, Art. no. 3327.
[5] L. Appeltant *et al.*, "Information processing using a single dynamical node as complex system," *Nature. Commun.*, vol. 2, no. 9, 2011, Art. no. 468.
[6] K. Yoshimura *et al.*, "Secure key distribution using correlated randomness in lasers driven by common random light," *Phys. Rev. Lett.*, vol. 108, no. 7, 2012, Art. no. 070602.
[7] Y. K. Chembo, D. Brunner, M. Jacquot, and L. Larger, "Optoelectronic oscillators with time-delayed feedback," *Rev. Mod. Phys.*, vol. 91, no. 3, 2019, Art. no. 035006.
[8] H. Gao *et al.*, "0.75 Gbit/s high-speed classical key distribution with mode-shift keying chaos synchronization of Fabry-Perot lasers," *Light: Sci. Appl.*, vol. 10, no. 1, pp. 1–9, 2021.
[9] C. H. Tseng, R. Funabashi, K. Kanno, A. Uchida, C. C. Wei, and S. K. Hwang, "High-entropy chaos generation using semiconductor lasers subject to intensity-modulated optical injection for certified physical random number generation," *Opt. Lett.*, vol. 46, no. 14, pp. 3384–3387, 2021.
[10] M. Virte, E. Mercier, H. Thienpont, K. Panajotov, and M. Sciamanna, "Physical random bit generation from chaotic solitary laser diode," *Opt. Exp.*, vol. 22, pp. 17271–17280, 2014.
[11] F. Y. Lin and J. M. Liu, "Chaotic lidar," *IEEE J. Sel. Topics Quantum Electron.*, vol. 10, no. 5, pp. 991–997, Sep./Oct. 2004.
[12] C. H. Cheng, C. Y. Chen, J. D. Chen, D. K. Pan, K. T. Ting, and F. Y. Lin, "3D pulsed chaos lidar system," *Opt. Exp.*, vol. 26, no. 9, pp. 12230–12241, 2018.
[13] M. Naruse *et al.*, "Scalable photonic reinforcement learning by time-division multiplexing of laser chaos," *Sci. Rep.*, vol. 8, no. 1, 2018, Art. no. 10890.
[14] H. H. Lu *et al.*, "A 56 Gb/s PAM4 VCSEL-based LiFi transmission with two-stage injection-locked technique," *IEEE Photon. J.*, vol. 9, no. 1, Feb. 2017, Art. no. 7900208.
[15] W. S. Tsai, H. H. Lu, Y. C. Huang, S. C. Tu, and Q. P. Huang, "A PDM-based bi-directional fibre-FSO integration with two RSOAs scheme," *Sci. Rep.*, vol. 9, no. 1, pp. 1–8, 2019.
[16] X. H. Huang, C. Y. Li, H. H. Lu, C. R. Chou, H. M. Hsia, and Y. H. Chen, "A bidirectional FSO communication employing phase modulation scheme and remotely injection-locked DFB LD," *J. Lightw. Technol.*, vol. 38, no. 21, pp. 5883–5892, 2020.

[17] Q. Tareq, A. M. Ragheb, M. A. Esmail, S. A. Alshebeili, and M. Z. M. Khan, "Performance of injection-locked quantum-dash MMW source under clear and dusty weather conditions," *IEEE Photon. J.*, vol. 13, no. 3, Jun. 2021, Art. no. 1500409.

[18] M. H. Chen, S. C. Hsiao, K. T. Shen, C. C. Tsai, and H. C. Chui, "Single longitudinal mode external cavity blue InGaN diode laser," *Opt. Laser Technol.*, vol. 116, pp. 68–71, 2019.

[19] M. H. M. Shamim *et al.*, "Analysis of optical injection on red and blue laser diodes for high bit-rate visible light communication," *Opt. Commun.*, vol. 449, pp. 79–85, 2019.

[20] H. Asghar, E. Sooudi, M. A. Baig, and J. G. McInerney, "Recent advances in stabilization of mode-locked quantum dash lasers at 1.55 μm by dual-loop optical feedback," *Opt. Laser Technol.*, vol. 122, 2020, Art. no. 105884.

[21] F. Grillot, J. Duan, B. Dong, and H. Huang, "Uncovering recent progress in nanostructured light-emitters for information and communication technologies," *Light: Sci. Appl.*, vol. 10, no. 1, 2021, Art. no. 156.

[22] M. C. Soriano, J. Garcia-Ojalvo, C. R. Mirasso, and I. Fischer, "Complex photonics: Dynamics and applications of delay-coupled semiconductors lasers," *Rev. Mod. Phys.*, vol. 85, Mar. 2013, Art. no. 421.

[23] Y. Deng *et al.*, "Mid-infrared hyperchaos of interband cascade lasers," *Light: Sci. Appl.*, vol. 11, no. 7, pp. 1–10, 2022.

[24] D. Rontani, A. Locquet, M. Sciamanna, and D. S. Citrin, "Loss of time-delay signature in the chaotic output of a semiconductor laser with optical feedback," *Opt. Lett.*, vol. 32, pp. 2960–2962, Oct. 2007.

[25] X. Z. Li and S. C. Chan, "Detection dependencies of statistical properties for semiconductor laser chaos," *IEEE J. Sel. Topics Quantum Electron.*, vol. 25, no. 6, Nov./Dec. 2019, Art. no. 1501209.

[26] Y. Chen *et al.*, "Unveil the time delay signature of optical chaos systems with convolutional neural network," *Opt. Exp.*, vol. 28, no. 10, pp. 15221–15231, 2020.

[27] P. Zhou, Q. Fang, and N. Li, "Phased-array assisted time-delay signature suppression in the optical chaos generated by an external-cavity semiconductor laser," *Opt. Lett.*, vol. 45, no. 2, pp. 399–402, 2019.

[28] G. Bouchez, T. Malica, D. Wolfersberger, and M. Sciamanna, "Optimized properties of chaos from a laser diode," *Phys. Rev. E*, vol. 103, 2021, Art. no. 042207.

[29] C. Xue, N. Jiang, Y. Lv, and K. Qiu, "Secure key distribution based on dynamic chaos synchronization of cascaded semiconductor laser systems," *IEEE Trans. Commun.*, vol. 65, no. 1, pp. 312–319, Jan. 2017.

[30] Z. Zhao *et al.*, "Semiconductor-laser-based hybrid chaos source and its application in secure key distribution," *Opt. Lett.*, vol. 44, no. 10, pp. 2605–2608, 2019.

[31] S. Sunada *et al.*, "Chaos laser chips with delayed optical feedback using a passive ring waveguide," *Opt. Exp.*, vol. 19, pp. 5713–5724, Mar. 2011.

[32] J. G. Wu *et al.*, "Direct generation of broadband chaos by a monolithic integrated semiconductor laser chip," *Opt. Exp.*, vol. 21, no. 20, pp. 23358–23364, 2013.

[33] J. G. Wu, G. Q. Xia, and Z. M. Wu, "Suppression of time delay signatures of chaotic output in a semiconductor laser with double optical feedback," *Opt. Exp.*, vol. 17, pp. 20124–20133, Oct. 2009.

[34] B. Cui *et al.*, "Generation of chaotic signals with concealed time-delay signature based on a semiconductor laser under multi-path optical feedback," *IEEE Photon. J.*, vol. 14, no. 1, Feb. 2022, Art. no. 1504605.

[35] S. Priyadarshi, Y. Hong, I. Pierce, and K. A. Shore, "Experimental investigations of time-delay signature concealment in chaotic external cavity VCSELs subject to variable optical polarization angle of feedback," *IEEE J. Sel. Topics Quantum Electron.*, vol. 19, no. 4, Jul./Aug. 2013, Art. no. 1700707.

[36] H. Lin, Y. Hong, and K. A. Shore, "Experimental study of time-delay signatures in vertical-cavity surface-emitting lasers subject to double-cavity polarization-rotated optical feedback," *J. Lightw. Technol.*, vol. 32, pp. 1829–1836, 2014.

[37] S. S. Li, Q. Liu, and S. C. Chan, "Distributed feedbacks for time-delay signature suppression of chaos generated from a semiconductor laser," *IEEE Photon. J.*, vol. 4, no. 5, pp. 1930–1935, Oct. 2012.

[38] Z. Q. Zhong, S. S. Li, S. C. Chan, G. Q. Xia, and Z. M. Wu, "Polarization-resolved time-delay signatures of chaos induced by FBG-feedback in VCSEL," *Opt. Exp.*, vol. 23, pp. 15459–15468, 2015.

[39] Y. Xu, M. Zhang, L. Zhang, P. Lu, and X. Bao, "Time-delay signature suppression in a chaotic semiconductor laser by fiber random grating induced distributed feedback," *Opt. Lett.*, vol. 42, no. 20, pp. 4107–4110, 2017.

[40] J. Ke, L. Yi, T. Hou, Y. Hu, G. Xia, and W. Hu, "Time delay concealment in feedback chaotic systems with dispersion in loop," *IEEE Photon. J.*, vol. 9, no. 2, Apr. 2017, Art. no. 7200808.

[41] D. Wang *et al.*, "Time delay signature elimination of chaos in a semiconductor laser by dispersive feedback from a chirped FBG," *Opt. Exp.*, vol. 25, no. 10, pp. 10911–10924, 2017.

[42] N. Jiang, Y. Wang, A. Zhao, S. Liu, and K. Qiu, "Simultaneous bandwidth-enhanced and time delay signature-suppressed chaos generation in semiconductor laser subject to feedback from parallel coupling ring resonators," *Opt. Exp.*, vol. 28, no. 2, pp. 1999–2009, 2020.

[43] R. M. Nguimdo, M. C. Soriano, and P. Colet, "Role of the phase in the identification of delay time in semiconductor lasers with optical feedback," *Opt. Lett.*, vol. 36, pp. 4332–4334, Nov. 2011.

[44] R. M. Nguimdo, G. Verschaffelt, J. Danckaert, and G. Van derSande, "Loss of time-delay signature in chaotic semiconductor ring lasers," *Opt. Lett.*, vol. 37, pp. 2541–2543, Jun. 2012.

[45] H. Han, X. M. Cheng, Z. W. Jia, and K. A. Shore, "Suppression of cavity time-delay signature using noise-phase-modulated feedback," *IEEE Access*, vol. 8, pp. 35344–35349, 2020.

[46] B. Liu, S. Zhang, X. Zhang, and T. Wu, "Time-delay signature cancellation and bandwidth enhancement based on phase modulation injectionusing chaotic signals," *Appl. Opt.*, vol. 60, no. 17, pp. 5245–5251, 2021.

[47] A. P. A. Fischer, M. Yousefi, D. Lenstra, M. W. Carter, and G. Vemuri, "Filtered optical feedback induced frequency dynamics in semiconductor lasers," *Phys. Rev. Lett.*, vol. 92, no. 2, pp. 023901.1–023901.4, 2004.

[48] C. Xue, S. Ji, A. Wang, N. Jiang, and K. Qiu, "Narrow-linewidth single-frequency photonic microwave generation in optically injected semiconductor lasers with filtered optical feedback," *Opt. Lett.*, vol. 43, no. 17, pp. 4184–4187, 2018.

[49] S. S. Li, X. Zou, L. Wang, A. Wang, W. Pan, and L. Yan, "Stable period-one oscillations in a semiconductor laser under optical feedback from a narrowband fiber Bragg grating," *Opt. Exp.*, vol. 28, no. 14, pp. 21286–21299, 2020.

[50] R. Lang and K. Kobayashi, "External optical feedback effects on semiconductor injection laser properties," *IEEE J. Quantum Electron.*, vol. QE-16, no. 3, pp. 347–355, Mar. 1980.

[51] S. S. Li and S. C. Chan, "Chaotic time-delay signature suppression in a semiconductor laser with frequency-detuned grating feedback," *IEEE J. Select. Topics Quantum Electron.*, vol. 21, no. 6, pp. 541–552, Nov./Dec. 2015.

[52] S. K. Hwang, J. M. Liu, and J. K. White, "35-Ghz intrinsic bandwidth for direct modulation in 1.3-μm semiconductor lasers subject to strong injection locking," *IEEE Photon. Technol. Lett.*, vol. 16, no. 4, pp. 972–974, Apr. 2004.

[53] J. M. Liu, *Photonic Devices*. Cambridge, U.K.: Cambridge Univ. Press, 2009.

[54] T. Erdogan, "Fiber grating spectra," *J. Lightw. Technol.*, vol. 15, no. 8, pp. 1277–1294, 1997.

[55] D. Lenstra, B. H. Verbeek, and A. Den Boef, "Coherence collapse in single-mode semiconductor lasers due to optical feedback," *IEEE J. Quantum Electron.*, vol. QE-21, no. 6, pp. 674–679, 1985.

[56] S. C. Chan, "Analysis of an optically injected semiconductor laser for microwave generation," *IEEE J. Quantum Electron.*, vol. 46, no. 3, pp. 421–428, Mar. 2010.

[57] F. Y. Lin, Y. K. Chao, and T. C. Wu, "Effective bandwidths of broadband chaotic signals," *IEEE J. Quantum Electron.*, vol. 48, no. 8, pp. 1010–1014, Aug. 2012.